

Direct probing of the exchange interaction at buried interfaces

Kh. Zakeri^{1*}, T.-H. Chuang¹, A. Ernst^{1,2}, L. M. Sandratskii¹, P. Buczek¹, H. J. Qin¹, Y. Zhang^{1,3} and J. Kirschner^{1,4}

The fundamental interactions between magnetic moments at interfaces have an important impact on the properties of layered magnetic structures. Hence, a direct probing of these interactions is highly desirable for understanding a wide range of phenomena in low-dimensional solids. Here we propose a method for probing the magnetic exchange interaction at buried interfaces using spin-polarized electrons and taking advantage of the collective nature of elementary magnetic excitations (magnons). We demonstrate that, for the case of weak coupling at the interface, the low-energy magnon mode is mainly localized at the interface. Because this mode has the longest lifetime of the modes and has a finite spectral weight across the layers on top, it can be probed by electrons. A comparison of experimental data and first-principles calculations leads to the determination of the interface exchange parameters. This method may help the development of spectroscopy of buried magnetic interfaces.

Magnons are the elementary magnetic excitations in a magnetically ordered solid. Generally, each magnon corresponds to the reduction in the total magnetization of the system by two Bohr magnetons ($2\mu_B$), which is manifested as the deviation of the atomic moments from the equilibrium direction. There are a few important differences between magnon excitations in thin films grown on a substrate and those in bulk crystals. In single-element bulk crystals all atoms are equivalent and contribute equally to different magnon modes. This means that a magnon can be visualized as the deviation of all atomic moments by the same angle θ from the equilibrium direction, whereas the variation of the azimuth angle ϕ is defined by the wavevector of the magnon. All moments precess with the same eigenfrequency about the equilibrium direction. The eigenfrequency ω of the precession determines the energy of the magnons ($E = \hbar\omega$, where \hbar is the reduced Planck's constant).

However, in thin films, the atoms become inequivalent due to the absence of translational invariance in the direction orthogonal to the surface. Consequently, the atoms located in the surface and interface atomic layers have a smaller effective interatomic exchange coupling than the atoms located in the inner part of the film. Of particular interest is the strength of the coupling at the interface, because it has a direct impact on the properties of the system¹. For atoms located in the surface atomic layer, the important factor influencing the interatomic exchange interaction is the reduced atomic coordination. For atoms located in the interface atomic layer an additional strong influence comes from the hybridization of the electronic states of the atoms with those of the substrate atoms. A natural consequence of the inequivalence of the atomic layers is that the deviations of the moments θ characterizing a given magnon mode can differ for atoms located at different places in the structure^{2,3}. Hence, one can anticipate the existence of at least three different types of magnon: surface, bulk and interface magnons. In this nomenclature each magnon mode is named according to the part of the film whose atomic moments contribute most to that particular magnon mode. How different the surface and

interface magnons are in a given system depends strongly on the relative values of the interatomic exchange parameters at the surface, interface and bulk.

Generally, magnons can be excited and probed by different means, for example, neutrons, electrons and photons. Of these, electrons are the best for exciting magnons in small-sized structures, such as ultrathin films and nanostructures^{4–14}, because the interaction of electrons with the matter is much stronger than that with neutrons and photons. As a consequence, the spin-dependent inelastic mean free path in metallic ferromagnets is short^{15,16}. However, one has to take into account the most important feature of magnons in metallic systems. Different magnon modes have different spatial distributions across the film. Even those that are carrying the interface information have a finite spectral weight in the atomic layers on top. Moreover, the lifetime of different magnon modes is different. A competition between the spectral weight and the lifetime determines the experimental spectra. We will show that the low-energy magnon mode, localized mainly at the interface, has the longest lifetime of the modes, so a small spectral weight at the surface is sufficient to excite and probe this mode and thereby probe the interface exchange parameters.

Probing low-energy magnons in Fe(001) films on Ir(001)

As an example, we study the magnetic coupling at the interface of epitaxial thin Fe(001) films, six to nine atomic layers thick, grown on Ir(001). We use spin-polarized electron energy loss spectroscopy (SPEELS) to excite and probe the magnons. A schematic representation of the excitation and detection scheme in our experiment is presented in Fig. 1a. The Fe films investigated here are ferromagnetic at room temperature, as can be seen from the magnetic hysteresis loop presented in Fig. 1b. In SPEELS a well-defined spin-polarized electron beam is shot onto the sample surface, and the energy distribution of the scattered electrons is measured for two different spin polarizations of the incoming beam (parallel or antiparallel to the macroscopic magnetization). The difference spectrum is defined as $I_{\downarrow} - I_{\uparrow}$, where I_{\downarrow} and I_{\uparrow} are the recorded intensities of

¹Max-Planck-Institut für Mikrostrukturphysik, Weinberg 2, 06120 Halle, Germany, ²Wilhelm Ostwald Institut für Physikalische und Theoretische Chemie, Universität Leipzig, Linnéstrasse 2, 04103 Leipzig, Germany, ³Department of Chemistry, University College London, 20 Gordon Street, London WC1H 0AJ, UK, ⁴Institut für Physik, Martin-Luther-Universität Halle-Wittenberg, 06120 Halle, Germany. *e-mail: zakeri@mpi-halle.de

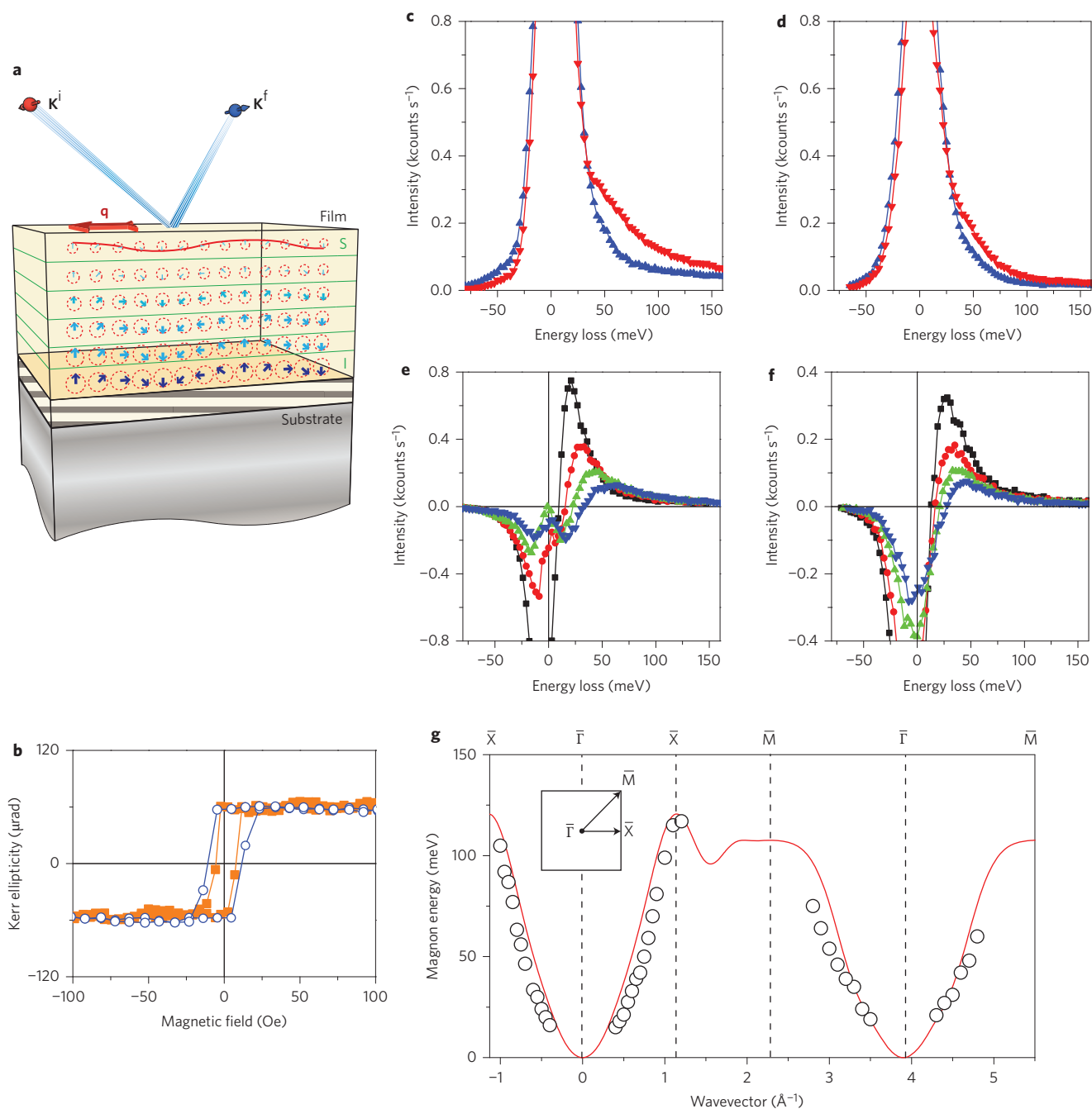


Figure 1 | Experimental scheme, magnetic hysteresis loop, typical spectra and magnon dispersion relation. **a**, Schematic representation of the SPEELS experiment. Small arrows in the atomic planes show the transverse component of the atomic magnetic moments precessing with eigenfrequency ω . Their length (radius of the precessing circle) indicates the amplitude of this particular magnon mode. The solid red line indicates the wave nature of these excitations. The low-energy magnon mode is mainly localized at the interface layer (I). It has a finite spectral weight at the surface layer (S). Magnons are excited by incidence of electrons of minority character. K^i and K^f are the momenta of electrons before and after the scattering process, respectively. q is the momentum of excited magnons. **b**, Typical magnetic hysteresis loops of a six-atomic-layer-thick Fe(001) film on Ir(001) recorded by the magneto-optical Kerr effect in longitudinal geometry with an external magnetic field applied along the $[1\bar{1}0]$ (solid squares) and $[0\bar{1}0]$ (open circles) directions. **c, d**, Typical SPEELS spectra recorded at an in-plane wavevector transfer of $\Delta K_{\parallel} = 0.8 \text{ \AA}^{-1}$ probed along the Fe[100] and Fe[110] directions, respectively. The intensity spectra I_{\downarrow} (red inverted triangles) and I_{\uparrow} (blue triangles) are obtained using the incident electrons with the spin parallel and antiparallel to the macroscopic magnetization, respectively. **e, f**, Series of difference spectra ($I_{\downarrow} - I_{\uparrow}$) at in-plane wavevector transfers of $\Delta K_{\parallel} = 0.5$ (black squares), 0.6 (red circles), 0.7 (green triangles) and 0.8 (blue inverted triangles) \AA^{-1} . Data recorded along the Fe[100] direction are presented in **e** and data recorded along the Fe[110] direction in **f**. **g**, Experimental (open symbols) and theoretical (solid curve) magnon dispersion relation. Only the low-energy mode is shown. The Brillouin zone is depicted in the inset.

scattered electrons when the spin polarization of the incoming electron beam is parallel and antiparallel to the magnetization, respectively. It carries all the information regarding the magnetic

excitations in the sample. The energy loss of electrons during the scattering process is equivalent to the energy of the excitation left behind in the sample. Owing to the fundamental conservation law

of total angular momentum during the scattering process, the creation of a magnon is only possible when the incoming electron is of spin-down character ($S = -\frac{1}{2}\hbar$, spin polarization parallel to the sample magnetization) and the scattered electron is of spin-up character ($S = +\frac{1}{2}\hbar$, antiparallel to the sample magnetization). In such a case, the total angular momentum of the sample decreases by \hbar , which is characteristic for a magnon¹⁷. The analysis of the difference spectra ($I_{\downarrow} - I_{\uparrow}$) provides direct information on the energy and lifetime of excited magnons^{14,18}. The conservation of parallel linear momentum during the scattering process accounts for the momentum of the excited magnons ($\Delta K_{\parallel} = q$, where $\Delta K_{\parallel} = K_{\parallel}^i - K_{\parallel}^f$ is the parallel momentum transfer of electrons to the sample and q is the momentum of the magnons).

Typical SPEELS spectra recorded on a six-atomic-layer-thick Fe film grown on Ir(001) at an in-plane wavevector transfer of $\Delta K_{\parallel} = 0.8 \text{ \AA}^{-1}$ are shown in Fig. 1c,d. The measurements performed along Fe[100] ($\bar{\Gamma}-\bar{X}$ in the reciprocal space) are presented in Fig. 1c and those along Fe[110] ($\bar{\Gamma}-\bar{M}$ in reciprocal space) in Fig. 1d. In this notation, $\bar{\Gamma}$ represents the centre, and \bar{X} and \bar{M} denote the high symmetry points of the Brillouin zone (see inset of Fig. 1g). Along both directions, the magnon peak is visible in the energy loss region of the minority channel. The magnon energies can be identified easily in the difference spectra, as shown in Fig. 1e,f. The peak position indicates the excitation energy. The magnon dispersion relation is constructed by plotting the magnon energies as a function of the wavevector for both probing directions (Fig. 1g). Surprisingly, the magnon energies are very low compared to those of bulk Fe. The length of the $\bar{\Gamma}-\bar{X}$ direction is 1.16 \AA^{-1} , and that of $\bar{\Gamma}-\bar{M}$ is 1.64 \AA^{-1} , assuming that the in-plane lattice constant of the Fe film is 2.72 \AA (this is because Fe grows pseudomorphically on an Ir(001) substrate, up to 10 atomic layers, with the epitaxial relationship Fe(110)||Ir(100))¹⁹. The data points of the measurement along the $\bar{\Gamma}-\bar{M}$ direction are only up to $\Delta K_{\parallel} = 1.1 \text{ \AA}^{-1}$. The reason for this is that the intensity of the difference spectra is too low for $\Delta K_{\parallel} > 1.1 \text{ \AA}^{-1}$ (Fig. 1f).

The low excitation energy and decreasing intensity of this mode with increasing number of Fe atomic layers from six to nine atomic layers (in particular close to the \bar{X} -point), without any substantial change in the energies, indicate that this mode is mainly localized at the interface (Supplementary Section S1). Obviously, for a surface magnon mode we would expect a very different behaviour, namely no significant change in the magnon intensity while increasing the number of atomic layers^{12,20}. The definite proof of this hypothesis comes from our first-principles calculations. We performed two different sets of calculations. The first set of calculations, accomplished with a self-consistent Green function method, yields the magnetic exchange parameters and magnon dispersion relation in an adiabatic approach and allows us to calculate the contribution of each atomic layer to the magnon modes. The second set of calculations, based on linear-response, time-dependent density functional theory, provides information on magnon lifetime. The low-energy mode, which satisfies the Goldstone theorem $E(q=0) = 0$, calculated for six atomic layers of Fe on Ir(001), is shown in Fig. 1g by the solid red line. The results of the calculations agree very well with the experimental results. Moreover, the calculated atomic- (or layer-) resolved transverse magnetic susceptibility results in the spatial distribution of each magnon mode over the Brillouin zone and allows us to compare the contribution of each atomic layer to each magnon mode.

Figure 2a shows the energies of all magnon modes calculated as the eigenvalues of the Heisenberg Hamiltonian. The susceptibility spectral functions projected into the interface and surface layers are presented in Fig. 2b and c, respectively. In this representation, the broadening of the lines indicates the contribution of the given layer to all magnon modes. For example, in Fig. 2b, the broadening of

the low-energy mode is much stronger than in the other modes, meaning that a large contribution into this mode comes from the Fe atoms located in the atomic layer next to the Ir(001) substrate. The zero energy of the uniform mode at $q=0$ reflects the fact that in the absence of the magnetic anisotropy the rigid reorientation of the magnetization of the system costs no energy, as expected from the Goldstone theorem. The change in the degree of localization with increasing wavevector is a complex process that depends on the pattern of the interatomic exchange parameters. Figure 2c shows the contribution of the surface layer to all magnon modes, indicating that the contribution of the surface layer to the low-energy mode is small for magnon wavevectors larger than 0.5 \AA^{-1} and is zero near the zone boundaries (near the \bar{X} - and \bar{M} -points). Because increasing the magnon wavevector means a larger angle ϕ between neighbouring atomic moments, the difference in the exchange parameters for different layers becomes increasingly more important, leading to the localization of the magnons in the region of the smallest exchange parameters. At $q=0$ (Goldstone mode), all atomic layers contribute equally to the low-energy mode. The contribution of the interface layer to this mode becomes larger as the wavevector increases, whereas the contributions from the other layers become smaller, such that at the \bar{X} point only the contribution of the interface atomic layer remains (Fig. 2d).

By conducting an independent experiment we estimated the average spin-dependent inelastic mean free path of Co film to be of the order of $\lambda \approx 4.5$ in the units of vertical layer spacing (being 1.6 \AA). If one assumes that Fe films have a similar spin-dependent mean free path one can estimate the expected intensity of the SPEELS spectra based on a simple kinematic model. As a rule of thumb, one may assume an exponential decay of the excitation probability with increasing deepness of the layer. Based on this assumption, the overall contribution of all layers to each magnon mode can be calculated as $A = \sum_{n=1}^6 A_n \exp(-l_{n,q}/\lambda)$, where A_n is the contribution of the n th layer to that particular magnon mode, n is the number of atomic layers counted from the top, and $l_{n,q}$ is the path length of electrons inside the film (which depends on n and q , or more precisely on the scattering geometry). The contribution of each layer to the low-energy mode taken from the *ab initio* calculations is presented in the upper panel of Fig. 2d. The quantity A is calculated as a function of the wavevector for the low-energy mode and is presented in the lower panel of Fig. 2d. It may be regarded as the expected intensity of the experimental difference spectra. Such a simple calculation reveals that the expected intensity close to the \bar{X} point is about 13% of that for $q=0.6 \text{ \AA}^{-1}$ in the middle of the $\bar{\Gamma}-\bar{X}$ direction. This means that, although at \bar{X} the main contribution to this mode is coming from the interface layer, it may still be measured by SPEELS. At this point we would like to mention that in this simple kinematic model only the probability of probing the interface mode is calculated; there are other parameters that may influence inelastic electron scattering that are not considered in this simple model.

Another way to illustrate that the low-energy mode is mainly localized at the interface is to calculate the magnon spectrum of the free-standing Fe(001) film. The results (Fig. 2e) show that the dispersion relation of the low-energy mode changes strongly, whereas the other modes are unaffected. For instance, the energy at \bar{X} is increased from 125 to 240 meV. Note that in this case the surface and interface layers are almost equivalent, so the spectral weights of the two low-energy modes projected into the surface and interface layers are almost identical. A comparison of Fig. 2b,c,e demonstrates the effect of hybridization of the electronic states of the film with those of the substrate on the magnon dispersion relation. It further illustrates how the degeneracy of the two low-energy magnon modes along the $\bar{X}-\bar{M}$ direction is broken and a mode with a lower energy is formed. This

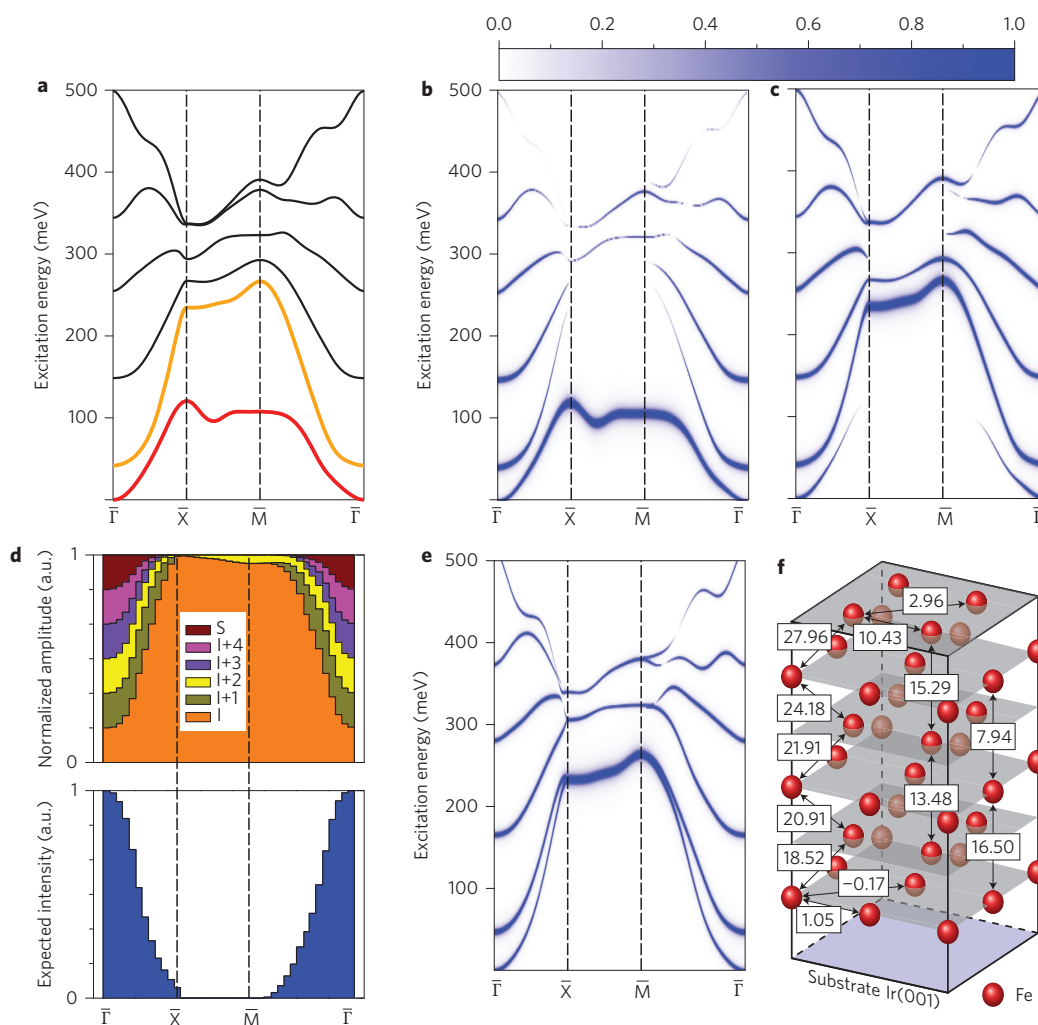


Figure 2 | Calculated magnon dispersion relation and spectral density for six atomic layers of Fe film on Ir(001) and site-resolved exchange coupling. **a**, Different magnon modes (black lines) obtained as eigenvalues of the Heisenberg Hamiltonian. The low-energy mode is shown in red, and the second mode in yellow. **b, c**, Atomic-resolved spectral function of the transverse susceptibility for atoms located in the interface (**b**) and surface (**c**) layers. The colour bar represents the normalized spectral weight. In this representation the broadening of the lines indicates the contribution of the given layer to all magnon modes. The low-energy mode has the highest spectral weight in the interface layer and hence is mainly localized at the interface. **d**, Top: contributions of each atomic layer to the low-energy magnon mode. S and I indicate surface and interface layers, respectively. Bottom: expected intensity of this mode when an averaged spin-dependent mean free path of 4.5 (in the unit of vertical layer spacing) is taken into account. **e**, Surface spectral function of the transverse susceptibility of six free-standing slabs of Fe(001) in vacuum. See colour bar in **b** and **c**. In this case, due to the symmetry of the system, the surface and interface layers have an equivalent spectral weight. **f**, Calculated interatomic exchange parameters. Values are given in milli-electronvolts (meV).

lowest-energy mode is mainly localized at the atomic layer next to the substrate, where the exchange parameters are weaker.

Determination of magnetic exchange parameters

The localization of magnons at the Fe/Ir(001) interface can be understood on the basis of an analysis of exchange parameters. In principle, the reduction of the coordination number at surfaces/interfaces can lead to magnon softening²⁰. However, in many systems, interface electronic properties are different from surface ones. This leads to a significant difference in the exchange parameters at the surface and at the interface. Remarkably, at the Fe/Ir(001) interface, magnon softening induced by interface hybridization is much more significant than that from the surface, which indicates a strong reduction in the intralayer exchange constants at the Fe/Ir(001) interface. Figure 2f shows the exchange parameters in the Fe/Ir(001) system. For simplicity, only the relevant parameters are presented. The interaction between atoms of the same atomic plane is referred to as intralayer coupling and that between

atoms from different layers is referred to as interlayer coupling. Although interlayer coupling for both surface and interface layers is strongly ferromagnetic, the intralayer exchange parameters are relatively small. In particular, the intralayer exchange parameters at the Fe/Ir interface have a strong tendency to be antiferromagnetic. Because of the strong ferromagnetic coupling between the layers, the ground state is still ferromagnetic.

The lifetime of different magnon modes

Another aspect that is of primary importance is the damping mechanism of the high-wavevector magnons, which is governed by the decay of the collective magnons into single-particle Stoner excitations^{14,18,21}. This type of damping, commonly referred to as Landau damping, is very strong in ferromagnetic metals and, as a rule, quickly increases with increasing magnon energy. As a result, for each wavevector q , only the lowest-energy magnon mode has a longer lifetime and can be unambiguously detected in the experiment. The contribution of all other magnon modes is

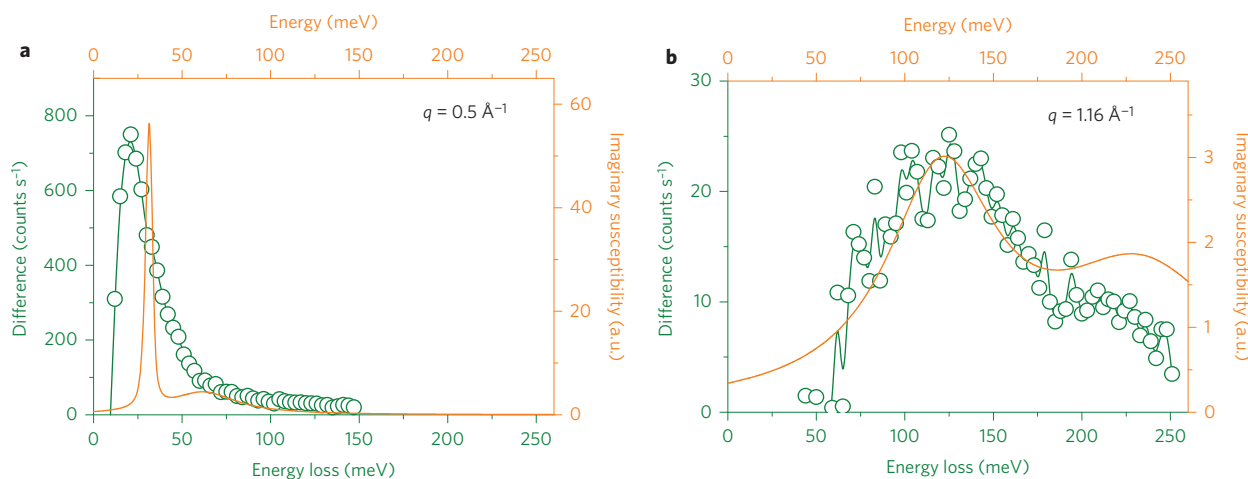


Figure 3 | Lifetime of different magnon modes. **a, b.** Comparison of SPEELS difference spectra, recorded at the middle (**a**, $\Delta k_{\parallel} = q = 0.5 \text{ \AA}^{-1}$) and edge (**b**) of the Brillouin zone ($\Delta k_{\parallel} = q = 1.16 \text{ \AA}^{-1}$, \bar{X} point), and corresponding calculated imaginary part of the dynamical spin susceptibility. The low-energy mode has the longest lifetime.

drastically reduced because of their strong damping (short lifetime). Competition between the spectral weight of different magnon modes and their damping determines the SPEELS response function. As discussed above, the amplitude of the interface magnons in the upper layers remains significant, but the damping of higher-energy magnons is very strong. Although the spectral weight of the interface mode is not as large as the surface mode, it has a much longer lifetime and hence dominates the spectra.

Calculation of the dynamic transversal spin susceptibility considers, on an equal footing, both collective magnons and single-electron Stoner excitations, and provides a full account of the Landau damping of the magnons. These calculations are presented in Fig. 3, which already shows drastic Landau damping of the higher energy magnon mode. Interestingly, a similar weak peak is observed in the experimental spectra, again showing good correlation between experiment and theory, even in such non-trivial features as the observation of strongly damped magnons. Without first-principles calculations of the dynamic spin susceptibility, noticing and interpreting this weak feature would have been virtually impossible.

Conclusions

For further illustration of the capability of this method for probing the interface exchange interaction, we replaced the top five Fe atomic layers with three atomic layers of Co (keeping only one atomic layer of Fe at the interface). The measured magnon dispersion relation revealed a very similar low-energy magnon mode, indicating that this mode originates mainly from the buried Fe atomic layer located at the interface (Supplementary Section S2).

The method illustrated above is also applicable to other ferromagnetic thin films grown on other substrates. If the magnetic coupling at the interface is weaker than at the surface, the low-energy magnon mode is localized mainly at the interface. If the interatomic exchange parameters at the interface and surface are similar, the surface and interface modes will have similar energies and also a very similar spectral weight. In such cases, by comparing the experimental results with the first-principles calculations, one can determine which magnon mode is observed in the experiment. The analysis would provide the values of the exchange parameters at both the surface and the interface.

The method is more easily applicable to cases where the coupling at the interface is weaker than at the surface. This leads to the clear separation of the low-energy magnon mode from the other modes. We calculated the magnon spectral density for Fe(001) films on Rh(001) and also for Co films on Cu(001) (Supplementary

Section S3). For the Co(001)/Cu(001) system the surface and interface layers make a very similar contribution to the low-energy magnon mode. Interestingly, for the Fe(001)/Rh(001) system, similar to Fe(001)/Ir(001), the low-energy magnon mode is mainly localized at the interface. The results demonstrate the degree of electronic hybridization of the film and substrate in these systems, which for the case of Co(001)/Cu(001) is rather weak but for Fe(001)/Ir(001) and Fe(001)/Rh(001) is very strong.

Methods

Experiment. All experiments were performed under ultrahigh vacuum. Before film deposition, the surface of the Ir(001) substrate was cleaned using our standard cleaning procedure (developed for refractory metals)²². This preparation resulted in a reconstructed Ir(001) – (5 × 1) surface. The reconstruction appears in two mutually orthogonal domains. The Fe films were grown by molecular beam epitaxy at 300 K and subsequently annealed at ~900 K to improve the surface quality. Low-energy electron diffraction showed very sharp (1 × 1) patterns, indicating a very well-ordered surface structure.

The magnetic state of the films was checked by means of the magneto-optical Kerr effect. The room-temperature ferromagnetic hysteresis loop is observed only for films with a thickness of more than five atomic layers. Recent theoretical calculations predict that the ground state of Fe films on Ir(001) for film thicknesses up to four atomic layers is a non-collinear magnetic ground state²³. Therefore, we chose a nominal thickness of six atomic layers as the starting point for our SPEELS measurements. Because Fe/Ir(001) shows a strong dependence of its magnetic properties on the number of Fe layers, one would expect that this crossover in the type of magnetic structure is the result of the difference in exchange parameters at the interface and in the inner atomic layers. We showed that this is indeed the case.

Longitudinal magneto-optical Kerr effect measurements performed on a six-atomic-layer-thick Fe film with the field applied along the [110] and [010] directions are presented in Fig. 1b. The two similar rectangular hysteresis loops indicate that the magnetic anisotropy of the film is very small. This would allow saturation of the magnetization of the film along any in-plane direction. The magnons are probed along a direction perpendicular to the magnetization. The sample was magnetized before the SPEELS measurements.

The SPEELS spectra were recorded at the remanent state. The scattering plane was chosen to be parallel to the Fe[100] (or Fe[110]) direction. The incident electron energy was 6 eV with an energy resolution of 16.9 meV. Along both directions, the magnon peak is nicely visible in the energy loss region of the minority channel. Electrons with their spin parallel to the sample magnetization are referred to as minority electrons and those with spin polarization antiparallel to the sample magnetization are referred to as majority electrons. The desired wavevector is achieved by changing the scattering geometry, that is, by changing the angle between the incident and scattered beam with respect to the surface normal.

Theory. Two sets of calculations were performed. The first set of calculations was performed within the framework of a generalized gradient approximation of density functional theory²⁴. The structural parameters of Fe/Ir(001) were taken from the available experimental data¹⁹. These served as the input for self-consistent calculations of the electronic structure using the Green function method, specially designed for layered semi-infinite systems²⁵. The Heisenberg exchange constants

were obtained by using the magnetic force theorem, implemented within the Green function method²⁶.

The second set of calculations were performed based on linear-response, time-dependent density functional theory²¹. This type of calculation provides information on the lifetime of excitations.

Received 18 March 2013; accepted 20 August 2013;
published online 22 September 2013

References

- Nolting, F. *et al.* Direct observation of the alignment of ferromagnetic spins by antiferromagnetic spins. *Nature* **405**, 767–769 (2000).
- Mills, D. L. Surface corrections to the specific heat of ferromagnetic films. *Phys. Rev. B* **1**, 264–274 (1970).
- Costa, A. T., Muniz, R. B. & Mills, D. L. Spin waves and their damping in itinerant ultrathin ferromagnets: intermediate wave vectors. *Phys. Rev. B* **74**, 214403 (2006).
- Ibach, H. *et al.* A novel spectrometer for spin-polarized electron energy-loss spectroscopy. *Rev. Sci. Instrum.* **74**, 4089–4095 (2003).
- Ibach, H., Rajeswari, J. & Schneider, C. M. An electron energy loss spectrometer designed for studies of electronic energy losses and spin waves in the large momentum regime. *Rev. Sci. Instrum.* **82**, 123904 (2011).
- Vollmer, R., Etkorn, M., Kumar, P. S. A., Ibach, H. & Kirschner, J. Spin-polarized electron energy loss spectroscopy of high energy, large wave vector spin waves in ultrathin fcc Co films on Cu(001). *Phys. Rev. Lett.* **91**, 147201 (2003).
- Heinrich, A. J., Gupta, J. A., Lutz, C. P. & Eigler, D. M. Single-atom spin-flip spectroscopy. *Science* **306**, 466–469 (2004).
- Balashov, T., Takács, A. F., Wulfhekel, W. & Kirschner, J. Magnon excitation with spin-polarized scanning tunneling microscopy. *Phys. Rev. Lett.* **97**, 187201 (2006).
- Tang, W. X. *et al.* Large wave vector spin waves and dispersion in two monolayer Fe on *w*(110). *Phys. Rev. Lett.* **99**, 087202 (2007).
- Gao, C. L. *et al.* Spin wave dispersion on the nanometer scale. *Phys. Rev. Lett.* **101**, 167201 (2008).
- Prokop, J. *et al.* Magnons in a ferromagnetic monolayer. *Phys. Rev. Lett.* **102**, 177206 (2009).
- Zhang, Y. *et al.* Nonmonotonic thickness dependence of spin wave energy in ultrathin Fe films: experiment and theory. *Phys. Rev. B* **81**, 094438 (2010).
- Zakeri, K. *et al.* Asymmetric spin-wave dispersion on Fe(110): direct evidence of the Dzyaloshinskii–Moriya interaction. *Phys. Rev. Lett.* **104**, 137203 (2010).
- Zakeri, K., Zhang, Y., Chuang, T.-H. & Kirschner, J. Magnon lifetimes on the Fe(110) surface: the role of spin–orbit coupling. *Phys. Rev. Lett.* **108**, 197205 (2012).
- Hong, J. & Mills, D. L. Theory of the spin dependence of the inelastic mean free path of electrons in ferromagnetic metals: a model study. *Phys. Rev. B* **59**, 13840–13848 (1999).
- Hong, J. & Mills, D. L. Spin dependence of the inelastic electron mean free path in Fe and Ni: explicit calculations and implications. *Phys. Rev. B* **62**, 5589–5600 (2000).
- Zakeri, K. & Kirschner, J. in *Probing Magnons by Spin-Polarized Electrons* Ch. 7, 84–99 (Topics in Applied Physics Magnonics From Fundamentals to Applications 125, Springer, 2013).
- Zhang, Y., Chuang, T.-H., Zakeri, K. & Kirschner, J. Relaxation time of terahertz magnons excited at ferromagnetic surfaces. *Phys. Rev. Lett.* **109**, 087203 (2012).
- Martin, V. *et al.* Pseudomorphic growth of Fe monolayers on Ir(001)(1×1): from a fct precursor to a bct film. *Phys. Rev. B* **76**, 205418 (2007).
- Zakeri, K., Zhang, Y. & Kirschner, J. Surface magnons probed by spin-polarized electron energy loss spectroscopy. *J. Electron Spectrosc. Rel. Phenom.* <http://dx.doi.org/10.1016/j.elspec.2012.06.009> (in the press).
- Buczek, P., Ernst, A. & Sandratskii, L. M. Different dimensionality trends in the Landau damping of magnons in iron, cobalt, and nickel: time-dependent density functional study. *Phys. Rev. B* **84**, 174418 (2011).
- Zakeri, K., Peixoto, T., Zhang, Y., Prokop, J. & Kirschner, J. On the preparation of clean tungsten single crystals. *Surf. Sci.* **604**, L1–L3 (2010).
- Deák, A., Szunyogh, L. & Ujfalussy, B. Thickness-dependent magnetic structure of ultrathin Fe/Ir(001) films: from spin-spiral states toward ferromagnetic order. *Phys. Rev. B* **84**, 224413 (2011).
- Perdew, J. P., Burke, K. & Ernzerhof, M. Generalized gradient approximation made simple. *Phys. Rev. Lett.* **77**, 3865–3868 (1996).
- Lüders, M., Ernst, A., Temmerman, W. M., Szotek, Z. & Durham, P. J. *Ab initio* angle-resolved photoemission in multiple-scattering formulation. *J. Phys.* **13**, 8587–8606 (2001).
- Liechtenstein, A. I., Katsnelson, M. I., Antropov, V. P. & Gubanov, V. A. Local spin density functional approach to the theory of exchange interactions in ferromagnetic metals and alloys. *J. Magn. Magn. Mater.* **67**, 65–74 (1987).

Acknowledgements

A.E. acknowledges funding from the Deutsche Forschungsgemeinschaft (DFG priority programme SPP 1538 ‘Spin Caloric Transport’). The calculations were performed at the Rechenzentrum Garching of the Max Planck Society.

Author contributions

Kh.Z. supervised the project, conceived and planned the experiments, participated in the analysis of the experimental data and wrote the paper. T.-H.C. carried out the experiments and analysed the experimental data. A.E. and P.B. performed the theoretical calculations. A.E. analysed the theoretical results. L.M.S. participated in the analysis of the theoretical results, the development of the structure of the paper and in writing the paper. H.J.Q. performed one part of the experiments and analysed the experimental data. Y.Z. contributed to the experiments. J.K. supervised the project. All authors contributed to the discussion of the results and improving the manuscript.

Additional information

Supplementary information is available in the [online version](#) of the paper. Reprints and permissions information is available online at www.nature.com/reprints. Correspondence and requests for materials should be addressed to Kh.Z.

Competing financial interests

The authors declare no competing financial interests.